Nonlinear Position Control for Hover and Automatic Landing of UAVs

Xilin Yang, Matt Garratt and Hemanshu Pota

Abstract

This paper presents a disturbance attenuation controller for horizontal position stabilization for hover and automatic landings of a rotary-wing unmanned aerial vehicle (RUAV) operating close to the landing deck in rough seas. Based on a helicopter model representing aerodynamics during the landing phase, a nonlinear state feedback $\mathcal{H}_\infty$ controller is designed to achieve rapid horizontal position tracking in a gusty environment. Practical constraints including flapping dynamics, servo dynamics and time lag effect are considered. A high-fidelity closed-loop simulation using parameters of the Vario XLC gas-turbine helicopter verifies performance of the proposed horizontal position controller.The proposed controller not only increases the disturbance attenuation capability of the RUAV, but also enables rapid position response when gusts occur. Comparative studies show that the $\mathcal{H}_\infty$ controller exhibits performance improvement and can be applied to ship/RUAV landing systems.

I. Introduction

RUAVs are suitable for a variety of applications such as surveillance and reconnaissance, search and rescue, oceanographic studies and volcano observation, etc. There is also a growing desire to operate a RUAV from ships at sea which introduces new challenges owing to the adverse turbulence over the flight deck and the ship motion through waves. Operational flexibility, including vertical take-off and landing capability, hover at a desired height, longitudinal and lateral manoeuvre, makes the RUAV an indispensable platform to perform such operations.

The main challenge in fulfilling maritime landing tasks results from the complicated aerodynamic environment, which consists of wave-excited movement of the ship deck and turbulent gusts. The gusts

X. Yang is with the Australian Research Center for Aerospace Automation, Brisbane, 4009, Australia. M. Garratt and H. Pota are with the School of Engineering and Information Technology, University College, University of New South Wales, ACT, 2600, Australia. E-mail: watermelo1980@gmail.com; {m.garratt,h.pota}@adfa.edu.au

mainly come from the ship airwake, which is governed by a variety of factors composing the geometry of the ship superstructure, the intensity and relative direction of the natural wind and free-stream turbulence [1]. The RUAV hovering over a ship deck operates in a partial ground effect condition where both the magnitude of the rotor flow and the inflow distribution over the rotor disk vary greatly [2]. This phenomenon results in a considerable change in the aerodynamic loading of the rotor system, which may affect the RUAV control margins, autopilot workload and power margins [3]. Therefore, dynamic performance of the RUAV is deteriorated and pure feedback driven controllers fail to stabilize the position response. This difficulty justifies the need for a controller with gust-attenuation properties. In addition, for an automatic landing, the descent trajectory of the RUAV deviates greatly from the desired trajectory when strong gusts occur. This necessitates rapid and accurate tracking performance to avoid missing the landing deck. Therefore, fast position response is another requirement for the controller design to achieve a safe landing.

Helicopter control in a turbulent environment has received attention in some papers. Cheviron et al. [4] proposed a robust guidance and control scheme for an autonomous helicopter in the presence of wind gusts. In [4], a high-gain observer was used to reconstruct the unknown inputs, and time derivative of the inputs were assumed to be uniformly bounded. The controller in [4] was designed based on the robust backstepping technique. Martini et al. [5] addressed the problem of the control of a model-scale helicopter under wind gusts. The disturbances in their paper were purely vertical wind gusts with typical levels less than $1ms^{-1}$. Also, they presented an active disturbance-rejection control strategy where system states were constructed using a nonlinear state observer. Robust control of helicopters has also been discussed in a number of papers. Civita et al. [6] have succeeded in implementing an $\mathcal{H}_\infty$ loop-shaping controller on a Yamaha R-50 helicopter. It was reported that tracking performance was improved using this design approach. Yang et al. [7] designed 6-DOF $\mathcal{H}_\infty$ controllers for the helicopter hover control. The design procedure was decoupled and controllers were divided into two groups with one for translational motion and the other for rotational motion. They also extended the design methodology in the presence of parameter uncertainties [8], [9].In [10], an $\mathcal{H}_\infty$ flight control system was designed to improve helicopter stability, maneuverability and agility. The linear $\mathcal{H}_\infty$ design approach was applied to a linearized model of the helicopter dynamics, and its performance was evaluated in simulations when constraints on actuators were taken into account.

The present research is part of efforts devoted to developing a feasible procedure for landing a RUAV on moving platforms in rough seas. In a previous paper [11], a feedback-feedforward controller has been designed to achieve height control of the RUAV in a gusty environment, and flight tests have been

conducted to confirm its performance. In this work, our objective is to design a controller with disturbance attenuation properties and rapid horizontal position tracking performance. The underlying significance is that the gust effect on the trajectory following capability of the RUAV can be greatly reduced, and the landing deck can be accurately tracked. This work begins with establishing a nonlinear model which captures dynamics of the RUAV during landing operations. This nonlinear model considers high-order system dynamics and applies them to the process of controller design. Thus, the effects of unmodeled high-order dynamics which a linear controller cannot handle can be greatly reduced using the proposed controller based on the nonlinear model. The nonlinear $\mathcal{H}_\infty$ controller is developed to achieve gust attenuation and fast horizontal position tracking performance.The computational burden of this controller is small as it only needs to solve the Riccati equation once and uses the solution to iteratively compute the controller gain matrices. The $\mathcal{H}_\infty$ controller employs the optimal control gains for the first-order dynamics by solving the Riccati equation as well as control gains dealing with high-order dynamics. Thus it outperforms the traditional PID controllers. Also, the $\mathcal{H}_\infty$ controller can directly compute control gains without the need to calculate control gains for inner and outer loops separately on a trial and error basis. Simulation results demonstrate that the proposed controller can effectively attenuate gust disturbance and achieve rapid and accurate position tracking when gusts occur.

II. A Review of the Nonlinear $\mathcal{H}_\infty$ Controller Design

Consider a nonlinear system described as follows:

$$\dot{x} = f(x) + g_1(x)\omega + g_2(x)U_c \tag{1}$$

$$z_m = h(x) + l(x)U_c \tag{2}$$

where $x \in \mathbf{R}^n$ is system state, $\omega \in \mathbf{R}^{m_1}$ disturbance, and $U_c \in \mathbf{R}^{m_2}$ control inputs. $z_m \in \mathbf{R}^r$ is a penalty variable. Functions $f(x), g_1(x), g_2(x), h(x)$ and $l(x)$ are smooth functions defined in a neighborhood U_e of the origin in $\mathbf{R}^n$. It is assumed that $f(0) = 0,\ h(0) = 0$. The following assumptions are also made,

$$h^T(x)l(x) = 0 \quad l^T(x)l(x) = R_h \tag{3}$$

where R_h is a nonsingular constant matrix, and is chosen to be symmetric to facilitate controller design. The state feedback control law $U_c = k(x)$ is a locally defined smooth function satisfying $k(0) = 0$.

The nonlinear state feedback controller used for stabilization of RUAV horizontal motion is based on the control approach described in [12; 13; 14], which has the disturbance attenuation capability described as follows

$$\int_0^{T_e} z_m^T(s) z_m(s) ds \leq \gamma_h^2 \int_0^{T_e} \omega^T(s)\omega(s) ds \tag{4}$$

with the attenuation factor satisfying $0 < \gamma_h < 1$. The attenuation factor γ_h shows to what extent effect of the disturbance ω on the penalty variable z_m can be attenuated. Thus, the inequality (4) can be used as a measure of the disturbance attenuation capability of the controller.

The controller design problem is reduced to finding a state feedback law U_c and a positive semi-definite function $V(x)$ to satisfy the following inequality

$$V_x(f(x) + g_1(x)\omega + g_2(x)U_c) + \frac{1}{2} \parallel h(x) + l(x)U_c \parallel^2 - \gamma_h^2 \parallel \omega \parallel^2 \leq 0 \tag{5}$$

Here, V_x denotes the Jacobian matrix of $V(x)$.

In [12; 14], a Taylor series approach to finding the state feedback controller is proposed. This approach employs the Hamiltonian function in the form of

$$H(x, V_x, \omega, U_c) = V_x(f(x) + g_1(x)\omega + g_2(x)U_c) + \frac{1}{2}(\|h(x) + l(x)U_c\|^2 - \gamma_h^2\|\omega\|^2) \tag{6}$$

and the function $V(x)$ takes the following form

$$V(x) = \frac{1}{2}x^T \bar{P} x + \sum_{k=3}^{\infty} \bar{P}_k x^{[k]} \tag{7}$$

where $x^{[k]} = [x_1^k, x_1^{k-1}x_2, \cdots, x_1^{k-2}x_2^2, x_1^{k-2}x_2x_3, \cdots, x_n^k]^T, k \geq 1$. The key to the $\mathcal{H}_\infty$ controller is to derive an explicit procedure to obtain the matrix $\bar{P}$ and row vector $\bar{P}_k$ such that $V(x)$ consists of a quadratic term and a nonlinear part which employs the power of components of system states.

Due to the orthogonal relationship between $h(x)$ and $l(x)$ shown in Eq. (3), the Hamiltonian function is converted to the following form,

$$H(x, V_x, \omega, U_c) = V_x f(x) + \frac{1}{2}h^T(x)h(x) + \begin{bmatrix} V_x g_1 & V_x g_2 \end{bmatrix} \begin{bmatrix} \omega \\ U_c \end{bmatrix} + \frac{1}{2} \begin{bmatrix} \omega \\ U_c \end{bmatrix}^T \bar{R} \begin{bmatrix} \omega \\ U_c \end{bmatrix} \tag{8}$$

where

$$\bar{R} = \begin{bmatrix} -\gamma_h^2 I & 0 \\ 0 & R_h \end{bmatrix} \tag{9}$$

Let $(\alpha_1, \alpha_2)^T = (\omega, U_c)^T$ and make

$$\frac{\partial H(x, V_x, \alpha_1, \alpha_2)}{\partial \alpha_1} = 0 \quad \frac{\partial H(x, V_x, \alpha_1, \alpha_2)}{\partial \alpha_2} = 0 \tag{10}$$

Then it can be obtained that

$$\begin{bmatrix} \alpha_1 \\ \alpha_2 \end{bmatrix} = \begin{bmatrix} \alpha_1(x, V_x) \\ \alpha_2(x, V_x) \end{bmatrix} = \begin{bmatrix} \frac{1}{\gamma_h^2} g_1^T V_x^T \\ -R_h^{-1} g_2^T V_x^T \end{bmatrix} \tag{11}$$

and the following equation is satisfied if $V(x)$ takes the form of Eq. (7) [14]

$$H(x, V_x, \alpha_1, \alpha_2) = V_x f(x) + \frac{1}{2} h^T(x) h(x) + \frac{1}{2} V_x (\frac{g_1 g_1^T}{\gamma_h^2} - g_2 R_h^{-1} g_2^T) V_x^T = 0 \tag{12}$$

Then the Hamiltonian function $H(x, V_x, \omega, U_c)$ turns out to be [13]

$$H(x, V_x, \omega, U_c) = -\gamma_h^2 \|\omega - \alpha_1(x, V_x)\|^2 + \|U_c - \alpha_2(x, V_x)\|^2 \tag{13}$$

It is seen from Eq. (13) that the control law [14]

$$U_c = \alpha_2(x, V_x) = -R_h^{-1} g_2^T V_x^T \tag{14}$$

leads to $H(x, V_x, \omega, U_c) \leq 0$. Therefore, disturbance attenuation capability of the $\mathcal{H}_\infty$ controller is guaranteed.In the following sections, the explicit form of U_c for stabilization of RUAV horizontal motion will be derived. This involves an iterative procedure to compute matrix $\bar{P}$ and row vectors $\bar{P}_k, k = 3, 4, \cdots$.

III. A Nonlinear $\mathcal{H}_\infty$ Position Controller

A. Modeling of Helicopter Dynamics

The design of a disturbance attenuation controller depends greatly on the choice of typical working conditions expected and tractability of the control problem associated with the resultant control plants. Usually, hover state is a typical working condition, and stabilization of the hover state is a prerequisite for an automatic landing. Therefore, the control plant is established for the hover condition, where main rotor thrust T_{mr} and tail rotor thrust T_{tr} are constant. This is achieved using the feedback-feedforward controller for height control. A complete helicopter dynamic model can be found in [15], and the dynamic

model under investigation is

$$\dot{x}_b = u + d_1 \tag{15}$$

$$\dot{y}_b = v + d_2 \tag{16}$$

$$\dot{u} = r_c v - q w_c + \frac{X_h}{M_a} - g \sin\theta + d_3 \tag{17}$$

$$\dot{v} = -r_c u + p w_c + \frac{Y_h}{M_a} + g \cos\theta \sin(\phi + \phi_0) + d_4 \tag{18}$$

$$\dot{p} = k_1 pq + k_2 q r_c + k_3 L_h + k_4 N_h + d_5 \tag{19}$$

$$\dot{q} = k_5 p r_c + k_6 (r_c^2 - p^2) + k_7 M_h + d_6 \tag{20}$$

$$\dot{\phi} = p + (q \sin(\phi + \phi_0) + r_c \cos(\phi + \phi_0)) \tan\theta + d_7 \tag{21}$$

$$\dot{\theta} = q \cos(\phi + \phi_0) - r_c \sin(\phi + \phi_0) + d_8 \tag{22}$$

Here, (x_b, y_b) are horizontal positions, (u, v, w_c) and (p, q, r_c) are linear and angular velocities with the subscript c indicating that the yaw rate r_c and vertical velocity w_c are obtained from onboard sensors (inertial measurement unit and GPS). Control inputs are longitudinal flapping a_1 and lateral flapping b_1, and disturbance input is $d_{(\cdot)}$. The roll and pitch are denoted by ϕ and θ, and the offset ϕ_0 is added to establish the desired equilibrium point. The parameters $k_{(\cdot)}$ are listed as follows

$$\begin{aligned}
\xi &= I_{xx} I_{zz} - I_{xz}^2 & k_1 &= \frac{I_{xz}(I_{xx} - I_{yy} + I_{zz})}{\xi} \\
k_2 &= \frac{I_{zz}(I_{yy} - I_{zz}) - I_{xz}^2}{\xi} & k_3 &= \frac{I_{zz}}{\xi} \\
k_4 &= \frac{I_{xz}}{\xi} & k_5 &= \frac{I_{zz} - I_{xx}}{I_{yy}} \\
k_6 &= \frac{I_{xz}}{I_{yy}} & k_7 &= \frac{1}{I_{yy}}
\end{aligned}$$

where I_{xx}, I_{yy}, I_{zz} and I_{xz} are moments of inertia and product of inertia. External forces (X_h, Y_h, Z_h) and moments (L_h, M_h, N_h) acting on the RUAV take the form of

$$X_h = T_{mr} a_1 \tag{23}$$

$$Y_h = T_{mr} b_1 + T_{tr} \tag{24}$$

$$Z_h = -T_{mr} \tag{25}$$

$$L_h = k_\beta b_1 + T_{mr} D_{mz} b_1 + T_{tr} D_{tz} \tag{26}$$

$$M_h = (-k_\beta - T_{mr} D_{mz}) a_1 \tag{27}$$

$$N_h = \frac{P_{mr}}{\Omega} + T_{mr} D_{mx} b_1 + T_{tr} D_{tx} \tag{28}$$

where k_β is the center-spring rotor stiffness, Ω the main rotor angular speed, and P_{mr} the main rotor power. Geometry parameters of the Vario helicopter D_{mz}, D_{tz}, D_{mx} and D_{tx} are listed in Table II.

The main rotor flapping dynamics are described by

$$\dot{a}_1 = -q - \frac{a_1}{\tau_f} + \frac{1}{\tau_f}(\frac{\partial a_1}{\partial u}u + A_{lon}\delta_{lon}) \tag{29}$$

$$\dot{b}_1 = -p - \frac{b_1}{\tau_f} + \frac{1}{\tau_f}(\frac{\partial b_1}{\partial v}v + B_{lat}\delta_{lat}) \tag{30}$$

where $\tau_f = \frac{16}{\gamma\Omega}$ is main rotor time constant with γ denoting the lock number. A_{lon} and B_{lat} are effective steady-state longitudinal and lateral gains, δ_{lon} and δ_{lat} are longitudinal cyclic and lateral cyclic. The Dihedral effect is

$$\frac{\partial a_1}{\partial u} = \frac{2}{\Omega R}\left(\frac{8C_T}{\alpha\sigma} + \sqrt{\frac{C_T}{2}}\right) \tag{31}$$

$$\frac{\partial b_1}{\partial v} = -\frac{2}{\Omega R}\left(\frac{8C_T}{\alpha\sigma} + \sqrt{\frac{C_T}{2}}\right) \tag{32}$$

where R is main rotor radius, α lift curve slope, σ the solidity ratio, and C_T thrust coefficient.

Remark 1 *The main rotor thrust T_{mr} and tail rotor thrust T_{tr} are considered to be constant as heave motion and yaw motion are stabilized using the existing feedback-feedforward controller and PD controller. Thus, dynamic equations for $\dot{z}_b, \dot{w}_c$ and $\dot{r}_c$ are neglected.*

Remark 2 *The constant offset ϕ_0 is added to the system dynamics to establish the desired equilibrium point for rolling motion. This enables zero initial condition and facilitates the control design.*

Remark 3 *For helicopters flying at low speeds, control forces and moments are mainly generated by the main rotor and the tail rotor. Forces and moments from fuselage, empennage and vertical fin are very small and they can be neglected.*

Remark 4 *Control inputs in the controller design process are set to be longitudinal flapping and lateral flapping. They will be converted later into longitudinal cyclic and lateral cyclic for implementation.*

The following vectors are defined for the controller design,

$$x = [x_b, y_b, u, v, p, q, \phi, \theta]^T \in \mathbf{R}^8$$

$$\omega = [d_1, d_2, d_3, d_4, d_5, d_6, d_7, d_8]^T \in \mathbf{R}^8$$

$$U_c = [a_1, b_1]^T \in \mathbf{R}^2$$

RUAV attitudes are very small ($\phi, \phi_0, \theta, \psi < 5^o$) in normal flight. Using small angle approximation, the trigonometric functions can be simplified

$$\sin\theta \approx \theta,\ \cos\theta \approx 1,\ \tan\theta \approx \theta,\ \sin(\phi+\phi_0) \approx \phi+\phi_0,\ \cos(\phi+\phi_0) \approx 1$$

and helicopter dynamics in horizontal plane can be written in a compact form

$$\dot{x} = f(x) + g_1(x)\omega + g_2(x)U_c \tag{33}$$

$$z_m = h(x) + l(x)U_c \tag{34}$$

where

$$f(x) = \begin{bmatrix} u \\ v \\ r_c v - q w_c + \frac{T_{mr} a_1}{M_a} - g\theta \\ -r_c u + p w_c + \frac{T_{mr} b_1 + T_{tr}}{M_a} + g(\phi+\phi_0) \\ k_1 pq + k_2 q r_c + k_3(k_\beta b_1 + T_{mr} D_{mz} b_1 + T_{tr} D_{tz}) + k_4(\frac{P_{mr}}{\Omega} + T_{mr} D_{mx} b_1 + T_{tr} D_{tx}) \\ k_5 p r_c + k_6(r_c^2 - p^2) + k_7(-k_\beta - T_{mr} D_{mz}) a_1 \\ p + (q(\phi+\phi_0) + r_c)\theta \\ q - r_c(\phi+\phi_0) \end{bmatrix} \tag{35}$$

$$g_1(x) = I_8 \tag{36}$$

$$g_2(x) = \begin{bmatrix} 0 & 0 & \frac{T_{mr}}{M_a} & 0 & 0 & b_1 & 0 & 0 \\ 0 & 0 & 0 & \frac{T_{mr}}{M_a} & b_2 & 0 & 0 & 0 \end{bmatrix}^T \tag{37}$$

with

$$b_1 = k_7(-k_\beta - T_{mr} D_{mz}), \quad b_2 = k_3 k_\beta + k_3 T_{mr} D_{mz} + k_4 T_{mr} D_{mx} \tag{38}$$

The constant matrices $h(x)$ and $l(x)$ are given by the expressions

$$h(x) = \left[\begin{array}{cccc} x_1 & & & \\ & \delta \cdot x_2 & & \\ & & \ddots & \\ & & & \delta \cdot x_8 \\ \hline 0 & \cdots & \cdots & 0 \\ 0 & \cdots & \cdots & 0 \end{array}\right]_{10\times 8} \qquad l(x) = \left[\frac{O_{8\times 2}}{I_2}\right]_{10\times 2} \tag{39}$$

where δ is a non-negative real number for making the controller design trade-off. Dimensions of the system model are $n = 8$, $m_1 = 8$ and $m_2 = 2$.

IV. NONLINEAR $\mathcal{H}_\infty$ POSITION CONTROL OF THE RUAV

The design approach begins with Taylor series expansion of the nonlinear functions in Eq. (35)-(37),

$$f(x) = \sum_{i=1}^{\infty} A_i x^{(i)} = A_1 x + f^{[2+]}(x) \tag{40}$$

$$h(x) = \sum_{i=1}^{\infty} C_i x^{(i)} = C_1 x + h^{[2+]}(x) \tag{41}$$

$$g_1(x) = B_1 + g_1^{[1+]}(x) \tag{42}$$

$$g_2(x) = B_2 + g_2^{[1+]}(x) \tag{43}$$

where $f^{[2+]}(x), h^{[2+]}(x), g_1^{[1+]}(x)$ and $g_2^{[1+]}(x)$ are high-order expansions.

For the RUAV model Eq.(15)-(22), $f(x)$ has a third-order expansion, and the three terms A_1, A_2 and A_3 are written as follows

$$A_1 = \begin{bmatrix} 0 & 0 & 1 & 0 & 0 & 0 & 0 & 0 \\ 0 & 0 & 0 & 1 & 0 & 0 & 0 & 0 \\ 0 & 0 & 0 & r_c & 0 & -w_c & 0 & -g \\ 0 & 0 & -r_c & 0 & w_c & 0 & g & 0 \\ 0 & 0 & 0 & 0 & k_1 q & k_1 p + k_2 r_c & 0 & 0 \\ 0 & 0 & 0 & 0 & k_5 r_c - 2k_6 p & 0 & 0 & 0 \\ 0 & 0 & 0 & 0 & 1 & (\phi + \phi_0)\theta & q\theta & q(\phi + \phi_0) \\ 0 & 0 & 0 & 0 & 0 & 1 & -r_c & 0 \end{bmatrix}_{8\times 8}$$

where $A_2 \in \mathbf{R}^{8\times 64}$ and $A_3 \in \mathbf{R}^{8\times 512}$ are large sparse matrices with a small number of non-zero values. The non-zero elements with their indices are listed below

$$\begin{aligned} &A_2(5,38) = k_1 && A_2(5,45) = k_1 \\ &A_2(6,37) = -2k_6 && A_2(7,47) = \theta \\ &A_2(7,48) = \phi + \phi_0 && A_2(7,54) = \theta \\ &A_2(7,56) = q && A_2(7,62) = \phi + \phi_0 \\ &A_2(7,63) = q \\ &A_3(7,376) = 1 && A_3(7,383) = 1 \\ &A_3(7,432) = 1 && A_3(7,446) = 1 \\ &A_3(7,495) = 1 && A_3(7,502) = 1 \end{aligned}$$

and $A_i = 0$ for $i > 3$.

The functions $g_1(x)$ and $g_2(x)$ can be expanded to the first-order ($g_1^{[1+]}(x) = 0,\ g_2^{[1+]}(x) = 0$),

$$B_1 = B_1^0 = [B_{11}, \ldots, B_{18}] = I_8 \tag{44}$$

$$B_2 = B_2^0 = [B_{21}, B_{22}] \tag{45}$$

where

$$B_{21} = \left[\begin{array}{cccccccc} 0 & 0 & \frac{T_{mr}}{M_a} & 0 & 0 & b_1 & 0 & 0 \end{array} \right]^T \tag{46}$$

$$B_{22} = \left[\begin{array}{cccccccc} 0 & 0 & 0 & \frac{T_{mr}}{M_a} & b_2 & 0 & 0 & 0 \end{array} \right]^T \tag{47}$$

Also, the matrix $C_1 \in \mathbf{R}^{10\times 8}$ is a large matrix with a few non-zero elements and the high-order terms $h^{[2+]}(x) = 0$. These non-zero elements with their indices are

$$C_1(1,1) = 1, \quad C_1(j,j) = 0.1, \quad j = 2, \cdots, 8. \tag{48}$$

Here, the trade-off factor is chosen to be $\delta = 0.1$.

A. Linear Part of the $\mathcal{H}_\infty$ Controller

The linear part of the $\mathcal{H}_\infty$ controller can be treated as a linear quadratic regulator problem, and only first-order system dynamics are used. The solution $\bar{P}$ can be obtained after solving the algebraic Riccati equation described by

$$H_{px}^T \bar{P} + \bar{P} H_{px} + \bar{P} H_{pp} \bar{P} + H_{xx} = 0 \tag{49}$$

with the following definitions

$$H_{px} = A_1, \quad H_{xx} = C_1^T C_1, \quad H_{pp} = \frac{B_1 B_1^T}{\gamma_h^2} - B_2 R_h^{-1} B_2^T \tag{50}$$

The solution $\bar{P}$ is required to construct the controller.

Eq. (49) can be rearranged into standard $\mathcal{H}_\infty$-like Riccati equation form ($R_h = I_2$)

$$A_1^T \bar{P} + \bar{P} A_1 - \bar{P} \left[\begin{array}{cc} B_1 & B_2 \end{array} \right] \left[\begin{array}{cc} -\gamma_h^2 I_{m_1} & O_{m_1 \times m_2} \\ O_{m_2 \times m_1} & I_{m_2} \end{array} \right]^{-1} \left[\begin{array}{c} B_1^T \\ B_2^T \end{array} \right] \bar{P} + C_1^T C_1 = 0 \tag{51}$$

where $m_1 = 8, m_2 = 2$ and γ_h is the attenuation factor. Since the system model is controllable and observable, the unique positive semi-definite matrix $\bar{P}$ exists [16].

B. Nonlinear Part of the $\mathcal{H}_\infty$ Controller

The nonlinear part of the $\mathcal{H}_\infty$ controller involves iterative computation of several intermediate matrices. The resultant controller weighting matrices aim to deal with high-order dynamics of the helicopter.

1) Notation and Definitions: The following notations and definitions are introduced to facilitate the controller design

$$x^{(0)} = 1 \quad x^{(1)} = x \quad x^{(i)} = \underbrace{x \otimes x \otimes \cdots \otimes x}_{i \text{ factor}}, \ i = 2, 3, \cdots \tag{52}$$

where $\otimes$ is the Kronecker product. Constant matrices M_k and N_k can be used to set up the relationship between $x^{(k)}$ and $x^{[k]}$

$$x^{[k]} = M_k x^{(k)} \quad x^{(k)} = N_k x^{[k]} \tag{53}$$

where $M_k \in \mathbf{R}^{C(n_x,k) \times n_x^k}$ and $N_k \in \mathbf{R}^{n_x^k \times C(n_x,k)}$ satisfy

$$M_k N_k = I_{n_x}^{[k]} \tag{54}$$

Here, $I_{n_x}^{[k]}$ is an identity matrix of dimension

$$C(n_x, k) := C_{n_x+k-1}^k = \frac{\prod_{i=1}^k (n_x + k - i)}{k!} \tag{55}$$

The number of states is $n_x = 8$.

We adopt the following operator $row(A)$ which maps n by m matrix $A = (a)_{ij}$ to a 1 by mn row vector

$$row(A) = [a_{11}, a_{12}, \cdots, a_{1m}, \cdots, a_{n1}, \cdots, a_{nm}] \tag{56}$$

Also, for any integers $i \geq 1, k \geq i$, and row vector $\bar{P}_k^*$ of dimension n_x^k, there exists a matrix $\bar{P}_k^i \in \mathbf{R}^{n_x \times n_x^{k-1}}$ determined by $\bar{P}_k^*$ such that

$$\bar{P}_k^*(x^{(i-1)} \otimes I_{n_x} \otimes x^{(k-i)}) = (\bar{P}_k^i x^{(k-1)})^T \tag{57}$$

where $\bar{P}_k^*$ is partitioned to a 1 by n_x^i block matrix taking the form

$$\bar{P}_k^* = \left[P_{\underbrace{1 \cdots 11}_{i \ tuple}} \cdots P_{\underbrace{1 \cdots 1 n_x}_{i \ tuple}} \cdots P_{\underbrace{n_x \cdots n_x 1}_{i \ tuple}} \ P_{\underbrace{n_x \cdots n_x n_x}_{i \ tuple}} \right] \tag{58}$$

in which $P_{j_1, \cdots, j_i}, \ 1 \leq j_1, \cdots, j_i \leq n_x$ is a row vector of dimension n_x^{k-i}. The resultant matrix $\bar{P}_k^i$ is given by

$$\bar{P}_k^i = \begin{bmatrix} P_{\underbrace{1 \cdots 11}_{i \ tuple}} & P_{\underbrace{1 \cdots 21}_{i \ tuple}} & \cdots & P_{\underbrace{n_x \cdots n_x 1}_{i \ tuple}} \\ P_{\underbrace{1 \cdots 12}_{i \ tuple}} & P_{\underbrace{1 \cdots 22}_{i \ tuple}} & \cdots & P_{\underbrace{n_x \cdots n_x 2}_{i \ tuple}} \\ \vdots & \vdots & \vdots & \vdots \\ P_{\underbrace{1 \cdots 1 n_x}_{i \ tuple}} & P_{\underbrace{1 \cdots 2 n_x}_{i \ tuple}} & \cdots & P_{\underbrace{n_x \cdots n_x n_x}_{i \ tuple}} \end{bmatrix}$$

The controller design process is as follows [12]. Let $S_2 = \bar{P}$, and the following intermediate matrices are computed

$$W_{ij}^2 = row(S_2 B_{ij}^1);\ \ i = 1, 2; j = 1, ..., 8 \tag{59}$$

$$Y_{11}^1 = B_{11}^T S_2^T = B_{11}^T \bar{P} \tag{60}$$

$$E_3 = row(\bar{P} A_2) \tag{61}$$

$$F_3 = \sum_{l=1}^{2} (C_l^T C_{3-l}) = 0 \tag{62}$$

$$I_3^1 = \sum_{l=2}^{2} \sum_{j=1}^{8} row((W_{1j}^l)^T Y_{1j}^{3-l}) \tag{63}$$

$$I_3^2 = \sum_{j=1}^{2} row((W_{2j}^2)^T Y_{2j}^1) \tag{64}$$

Then,

$$H_3 = -(E_3 + \frac{F_3 - 2I_3^2}{2} + \frac{I_3^1}{\gamma_h^2}) N_3 = -E_3 N_3 \tag{65}$$

$$M_3 = x^{[3]} (x^{(3)})^{-1} \quad N_3 = x^{(3)} (x^{[3]})^{-1} \tag{66}$$

Also, the intermediate matrix U_3 is

$$U_3 = M_3 [\sum_{i=1}^{3} I_8^{(i-1)} \otimes \bar{T} \otimes I_8^{(3-i)}] N_3 \tag{67}$$

$$= M_3 [\bar{T} \otimes I_8^{(2)} + I_8^{(1)} \otimes \bar{T} \otimes I_8^{(1)} + I_8^{(2)} \otimes \bar{T}] N_3 \tag{68}$$

where

$$\bar{T} = H_{px} + H_{pp} \bar{P} \tag{69}$$

Then

$$\bar{P}_3 = H_3 U_3^{-1} \quad \bar{P}_3^* = \bar{P}_3 M_3 \quad S_3 = \sum_{i=1}^{3} (\bar{P}_3^i)^T \in \mathbf{R}^{64 \times 8} \tag{70}$$

The next step is to compute $\bar{P}_4$, which is $\bar{P}_4 = H_4 U_4^{-1}$. The following intermediate matrices are

calculated

$$E_4 = \sum_{l=2}^{3} row(S_l A_{5-l}) = row(\bar{P}A_3) + row(S_3 A_2) \tag{71}$$

$$F_4 = \sum_{l=1}^{3} row(C_l^T C_{4-l}) = 0 \tag{72}$$

$$Z_4 = row(S_3 H_{pp} S_3^T) \tag{73}$$

$$W_{ij}^3 = \sum_{l=2}^{3} row(S_l B_{ij}^{4-l}) = row(S_2 B_{ij}^2) + row(S_3 B_{ij}^2) \tag{74}$$

$$I_4^1 = \sum_{l=2}^{3} \sum_{j=1}^{8} row((W_{1j}^l)^T Y_{1j}^{4-l}) \tag{75}$$

$$G_4^1 = \sum_{l=2}^{2} \sum_{j=1}^{8} row((W_{1j}^l)^T W_{ij}^{4-l}) \tag{76}$$

$$I_4^2 = \sum_{l=2}^{3} \sum_{j=1}^{2} row((W_{2j}^l)^T Y_{2j}^{4-l}) \tag{77}$$

$$G_4^2 = \sum_{j=1}^{8} row((W_{2j}^2)^T W_{2j}^2) \tag{78}$$

$$M_4 = x^{[4]}(x^{(4)})^{-1} \in \mathbf{R}^{330\times 4096} \tag{79}$$

$$N_4 = x^{(4)}(x^{[4]})^{-1} \in \mathbf{R}^{4096\times 330} \tag{80}$$

Afterwards,

$$H_4 = -\frac{1}{2}(Z_4 + 2E_4)N_4 \tag{81}$$

The U_4 can be computed as

$$\begin{aligned} U_4 &= M_4[\sum_{i=1}^{4} I_8^{(i-1)} \otimes \bar{T} \otimes I_8^{(4-i)}]N_4 \\ &= M_4[\bar{T} \otimes I_8^{(3)} + I_8^{(1)} \otimes \bar{T} \otimes I_8^{(2)} + I_8^{(2)} \otimes \bar{T} \otimes I_8^{(1)} + I_8^{(3)}\bar{T}]N_4 \end{aligned} \tag{82}$$

Afterwards,

$$\bar{P}_4 = H_4 U_4^{-1} \quad \bar{P}_4^* = \bar{P}_4 M_4 \quad S_4 = \sum_{i=1}^{4} (\bar{P}_4^i)^T \in \mathbf{R}^{512\times 8} \tag{83}$$

The $\mathcal{H}_\infty$ controller takes the following form

$$U_c = (-R_h^{-1} B_2^T \bar{P})x + (-R_h^{-1} \begin{bmatrix} B_{21}^T S_3^T \\ B_{22}^T S_3^T \end{bmatrix} N_2)x^{[2]} + (-R_h^{-1} \begin{bmatrix} B_{21}^T S_4^T \\ B_{22}^T S_4^T \end{bmatrix} N_3)x^{[3]} \tag{84}$$

Here, intermediate matrices N_2 and N_3 are computed by Eq. (53), which are given by

$$N_2 = x^{(2)}(x^{[2]})^{-1} \qquad N_3 = x^{(3)}(x^{[3]})^{-1} \tag{85}$$

The key to this controller is to compute $\bar{P}_3$ and $\bar{P}_4$ (as shown in Eq. (70) and Eq. (83)), which are required to calculate S_3 and S_4 so that the nonlinear controller can be constructed. In the considered application, owing to the fact that system dynamics can only be expanded to the third-order, the proposed controller only contains state components up to the third-order and is described by Eq. (84) in terms of $x, x^{[2]}$ and $x^{[3]}$. The controller in Eq. (84) satisfies the disturbance attenuation property given in Eq. (4). For proof, interested readers can refer to [12; 14].

V. Simulation Results

A. Performance Evaluation of the $\mathcal{H}_\infty$ Controller

In this section, performance of the $\mathcal{H}_\infty$ controller is evaluated using parameters of the Vario helicopter shown in Table II. To make the results more applicable, servo dynamics are taken into account. Also, synchronization assessment is performed by adding pure lag into the closed-loop simulation. Furthermore, disturbance attenuation capability of the $\mathcal{H}_\infty$ controller is examined in a gusty environment and compared with a PID controller.

The longitudinal and lateral flapping commands given in Eq. (84) need to be converted into longitudinal and lateral cyclic for implementation. For the Vario helicopter, as the flapping reacts instantaneously, the longitudinal and lateral cyclic can be calculated using a closed-form linear solution given the desired flapping angles a_1^{des} and b_1^{des} generated by the $\mathcal{H}_\infty$ controller, i.e.,

$$\delta_{lon} = q\tau_f - a_1^{des} - \frac{\partial a_1}{\partial u}u \tag{86}$$

$$\delta_{lat} = -p\tau_f - b_1^{des} + \frac{\partial b_1}{\partial v}v \tag{87}$$

PID controllers have been widely applied due to their simplicity and effectiveness. In the considered application, height and yaw motion are stabilized using the feedforward and PD controllers. For the inner loop (roll and pitch) dynamics, two PD controllers are employed. Once control of inner loop is achieved, PID controllers are tuned for position and velocity (outer loop) control with the integral of the error signal eliminating undesired offsets.

The coupling effects between the inner loop and the outer loop of the helicopter dynamics make it challenging to tune PID control gains to achieve satisfactory responses. Simulations suggest that PID gains should be tuned separately. The strategy is to firstly tune control gains for altitude and yaw motion.

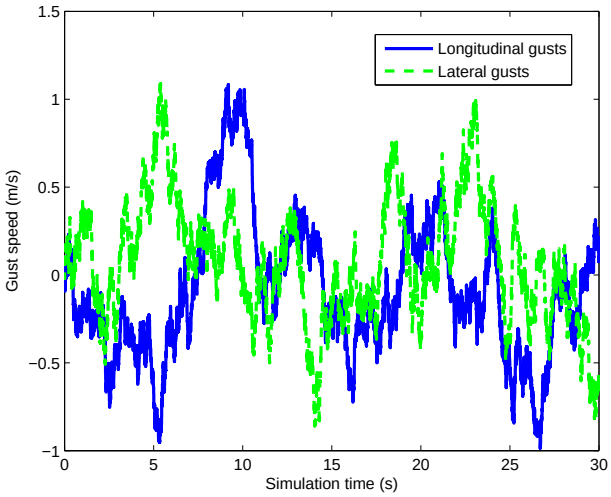

Fig. 1. Horizontal gusts used to test $\mathcal{H}_\infty$ controller

TABLE I

CONTROL GAINS FOR PID CONTROLLERS

	k_p	k_i	k_d
Altitude–PD	0.4	0	0.05
Yaw–PD	0.8	0	1.05
Roll–PD	-0.9	0	-0.5
Pitch–PD	0.5	0	0.1
Longitudinal–PD	-0.1	0	-0.1
Lateral–PID	0.05	0.005	0.2

Then, control of roll and pitch in the inner loop can be accomplished by repeating the same procedure. Afterwards, control gains in the outer loop are tuned while control gains in the inner loop are frozen. In the simulation, six PID controllers with the form

$$U_{PID} = k_p + \frac{k_i}{s} + k_d s \tag{88}$$

are selected with five PD controllers for altitude, yaw, roll, pitch and longitudinal position. A PID controller is used to remove offsets in lateral position.

To obtain the proper PID control gains, we empirically choose a group of gains which satisfy perfor-

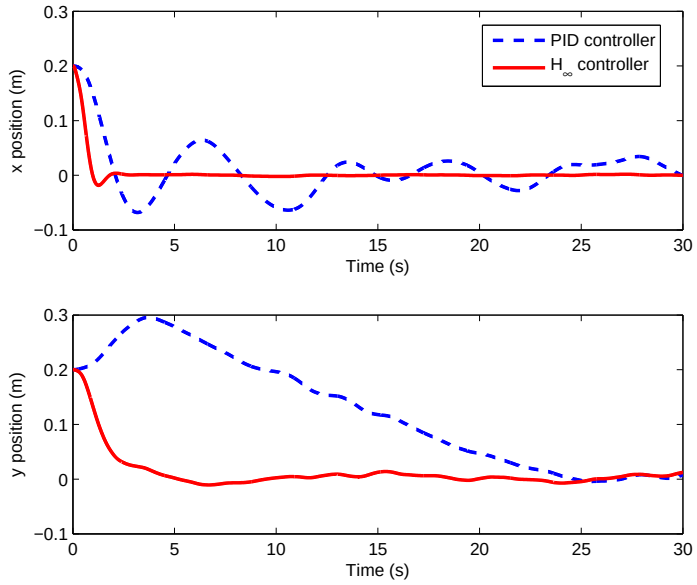

Fig. 2. Helicopter position response using PID controller and $\mathcal{H}_\infty$ controller

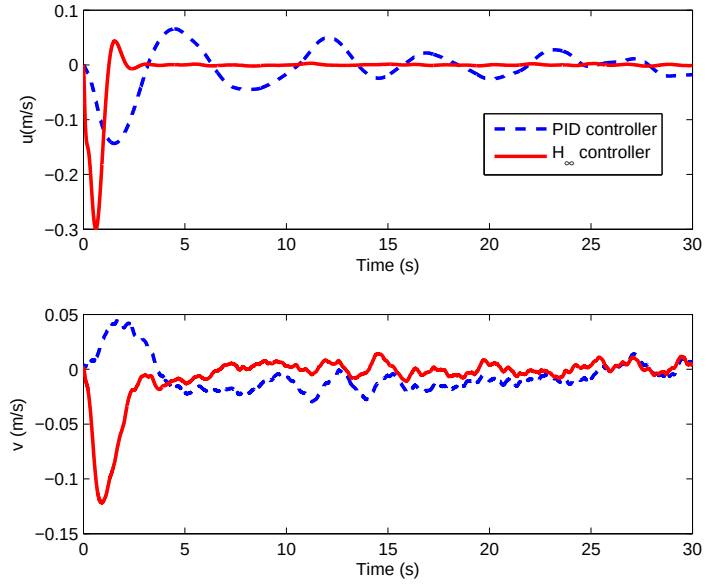

Fig. 3. Helicopter velocity response using PID controller and $\mathcal{H}_\infty$ controller

mance specifications such as settling time ($< 40s$) and steady-state error ($< \%5$ of reference signal). The integral of squared errors

$$J_e = J_{in} + J_{out} = \int_0^T [e_z^2(t) + e_\psi^2(t) + e_\theta^2(t) + e_\phi^2(t)]dt + \int_0^T [e_x^2(t) + e_y^2(t)]dt \tag{89}$$

provides a principle to choose the proper control gains. Here, J_{in} and J_{out} are integral of square errors of inner and outer loops, separately. Symbols $e_z, e_\psi, e_\theta, e_\phi, e_x, e_y$ are attitude and position errors. The proper PID control gains are selected such that they can reduce J_e greatly while exhibiting satisfactory transient response. Table I lists the suitable gains for comparison purposes.

For the $\mathcal{H}_\infty$ controller, exogenous disturbances are simulated using the *Dryden* gust model, as shown in Fig. 1. It is assumed that $\delta = 0.2$ and attenuation factor $\gamma_h = 6$. It takes $35.9s$ to compute the controller weighting matrices.

The horizontal position responses are shown in Fig. 2. It is noticed that positions x_b and y_b settle faster to the desired values $(x_b = 0, y_b = 0)$ from initial positions $(x_b = 0.2m, y_b = 0.2m)$ when the $\mathcal{H}_\infty$ controller is applied. The faster responses are the outcome of the rapid velocity responses depicted in Fig. 3. It takes more than $25s$ for the PID controller to attenuate gust effect to an acceptable level, and the oscillations in position cannot be damped completely. Control variables are shown in Fig. 4-5. The longitudinal cyclic using the $\mathcal{H}_\infty$ controller approaches that of the PID controller after $3s$. It is indicated in Fig. 5 that the $\mathcal{H}_\infty$ controller results in less oscillations in the lateral cyclic. Also, longitudinal and lateral cyclic are subject to larger transient response when the $\mathcal{H}_\infty$ controller is used. Thus for implementation of the $\mathcal{H}_\infty$ controller, more energy is required during the transient phase.

Several quantitative specification indices are employed to evaluate performance of the PID and the $\mathcal{H}_\infty$ controller, which consist of the maximum error ξ, the standard deviation σ and the overshoot λ. The index ξ is used to check the maximum error, σ aims to evaluate the deviation from the desired value, and λ is to assess the transient responses when different controllers are employed. The definitions of these specifications are listed as follows:

$$\xi = \max_i |X(i) - X_d| \tag{90}$$

$$\sigma = \sqrt{\frac{1}{N}\sum_{i=1}^{N}[X(i) - X_d]^2} \tag{91}$$

$$\lambda = |\frac{X_p - X_\infty}{X_\infty}| \tag{92}$$

Here, symbol X is the state to be evaluated (longitudinal position x_b or lateral position y_b), X_d desired state, X_p peak value of state, and X_∞ stable value of state. The number of states is denoted by N.

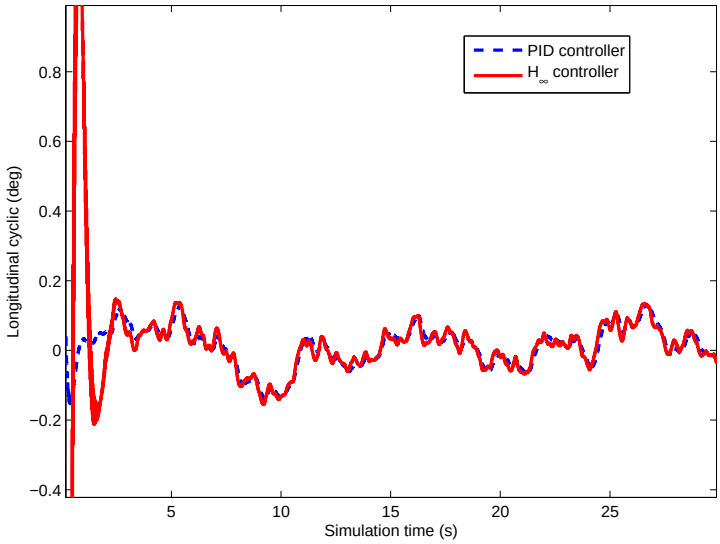

Fig. 4. Longitudinal cyclic commands using PID controller and $\mathcal{H}_\infty$ controller

To acquire a reliable performance evaluation of the PID and the $\mathcal{H}_\infty$ controllers, numerous simulations have been carried out for possible oncoming gusts, and performance of different controllers is illustrated in Fig. 6 for longitudinal position and Fig. 7 for lateral position. Here, 100 simulations were implemented with the sampling time of $0.5\ ms$, and desired positions were set to be $(x_b, y_b) = (10, 10)$. It is seen that both the maximum errors and standard deviation are much smaller when the $\mathcal{H}_\infty$ controller is applied. The proposed controller also keeps the overshoot at a small level and improves transient responses of helicopter position. The $\mathcal{H}_\infty$ controller employs optimal control gains by solving the Riccati equation as well as control gains dealing with high-order dynamics of the helicopter. Thus, it exhibits consistently better performance than the PID controller in a gusty environment. Another advantage of the $\mathcal{H}_\infty$ controller over the PID controller is the direct computation of control gains. It removes the need to compute control gains for inner and outer loops separately on the trial and error basis, which takes much effort to find the proper control gains.

B. Robustness Evaluation of the $\mathcal{H}_\infty$ Controller

In this section, robustness of the $\mathcal{H}_\infty$ controller is tested in consideration of servo dynamics and pure lag effect. It has been identified experimentally that servo dynamics can be approximated using the first-order transfer function with time constant τ_s [17; 18]. We tested the upper limit of τ_s that the

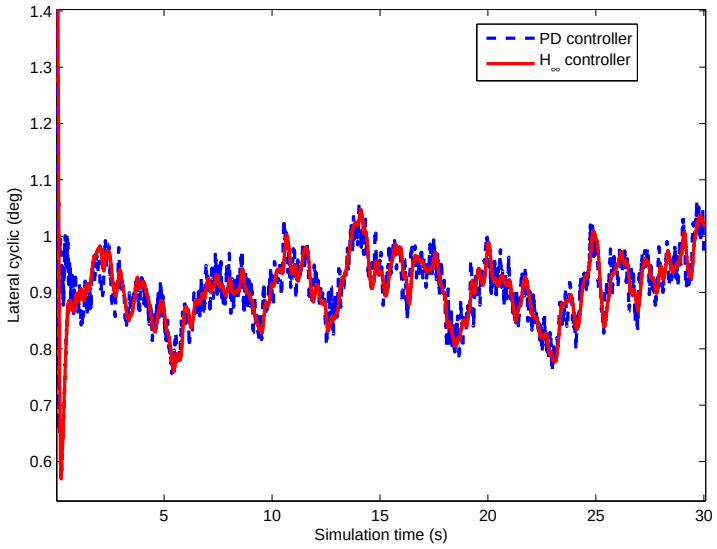

Fig. 5. Lateral cyclic commands using PID controller and $\mathcal{H}_\infty$ controller

$\mathcal{H}_\infty$ controller can tolerate. For the Vario helicopter, simulations show that the upper limit turns out to be $60ms$. In practice, performance of the controller is also affected by synchronization issues. This is essentially due to the fact that pure lags exist because sensor data arrive at different times. This is caused by transmitting, decoding and waiting until the next control update cycle. Therefore, a group of signals are required to wait for certain time in order to generate control commands in conjunction with other signals of late arrival. Pure lags are unavoidable when a controller is to be applied in practice. The simulations reveal that the $\mathcal{H}_\infty$ controller can tolerate a pure lag up to $30ms$. Although servo dynamics and pure lag effect are not considered when designing the $\mathcal{H}_\infty$ controller, the upper bounds from the simulations provide a clue on the requirement of implementing our controller.

VI. CONCLUSION

In this paper, a disturbance attenuation position controller is developed for RUAVs operating in a gusty environment. The horizontal positions are stabilized via a nonlinear state-feedback $\mathcal{H}_\infty$ controller. Performance of the proposed controller is evaluated through simulations in consideration of servo dynamics and pure lags. Comparative studies show that our controller can settle positions of the RUAV more rapidly than a PID controller in a gusty environment. Future work will focus on conducting flight tests of the $\mathcal{H}_\infty$ controller on the Vario helicopter.

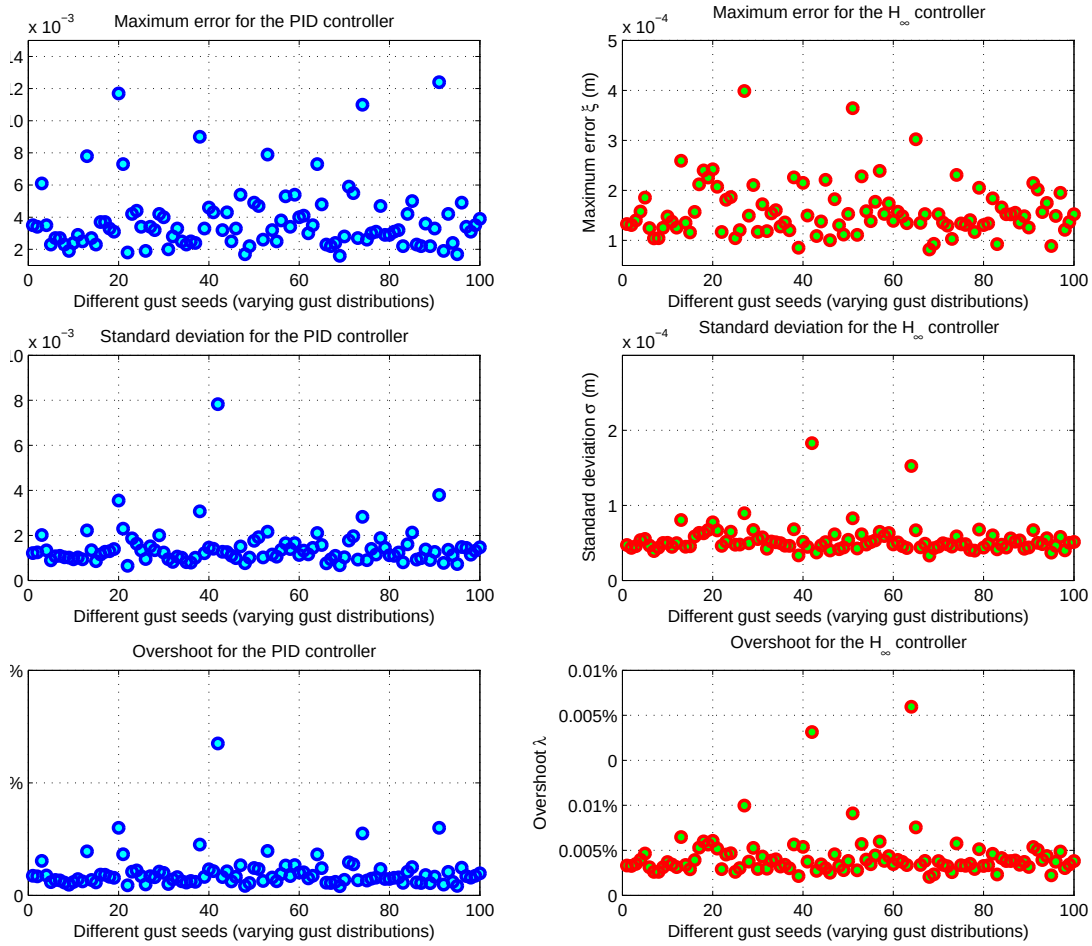

Fig. 6. Comparison of longitudinal positions x_b using PID controller and $\mathcal{H}_\infty$ controller

ACKNOWLEDGEMENT

The authors would like to thank Dr. Hamid Teimoori Sangani and Mr. Peter Leichsenring for useful discussions.

REFERENCES

[1] R. Fang and P. J. A. Booij, "Helicopter-ship qualification testing," in *the American Helicopter Society 62nd Annual Forum*, vol. 2, (Phoenix, Arizona), pp. 743–763, the American Helicopter Society International, Inc., May 2006.

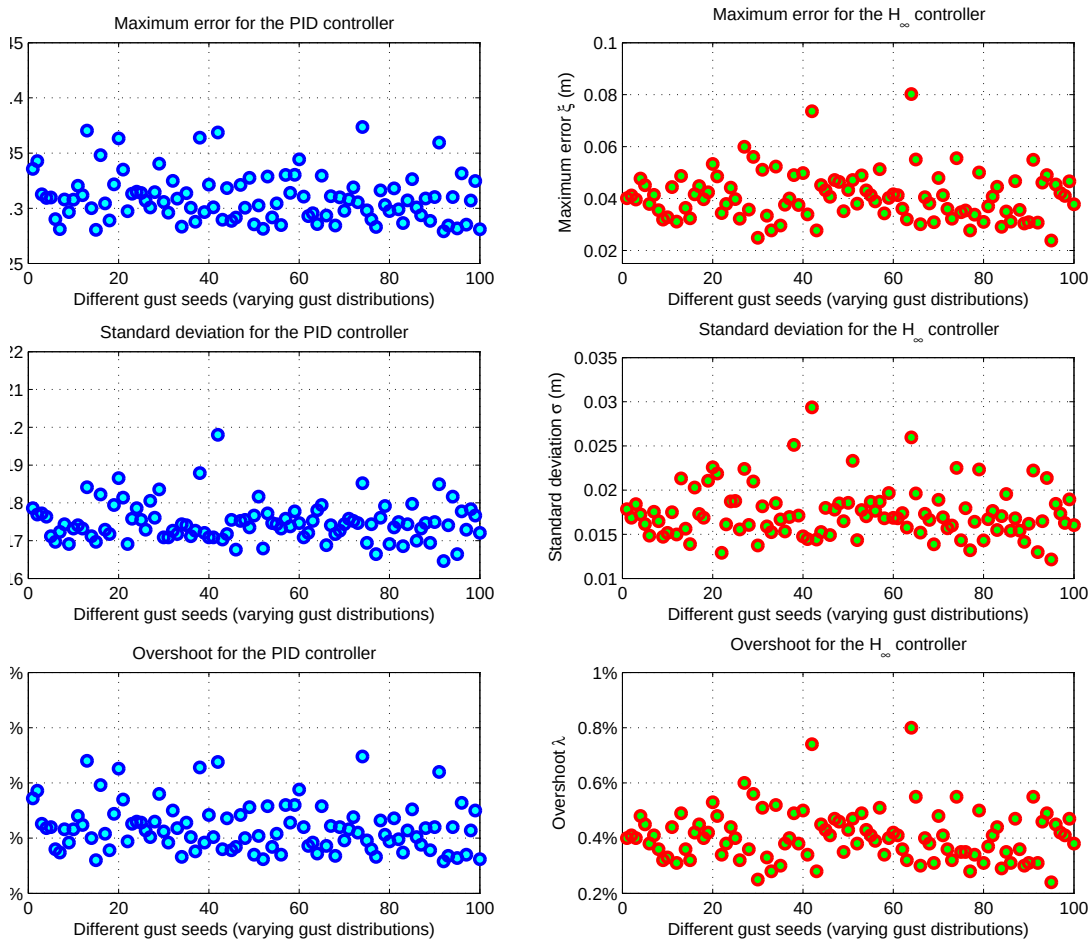

Fig. 7. Comparison of lateral positions y_b using PID controller and $\mathcal{H}_\infty$ controller

[2] H. Xin, C. He, and J. Lee, "Combined finite state rotor wake and panel ship deck models for simulation of helicopter shipboard operations," in *American Helicopter Society 57th Annual Forum*, vol. 2, (Washington, DC, USA), pp. 1187–1200, American Helicopter Society, May 2001.

[3] R. Toffoletto, R. Reddy, and J. Lewis, "Effect of ship frontal shape variation on flow field in flight deck region," in *Proceedings of the 2nd International Conference on Computational Fluid Dynamics, ICCFD*, (Sydney, Australia), 15-19th, Jul. 2002.

[4] T. Cheviron, F. Plestan, and A. Chriette, "A robust guidance and control scheme of an autonomous scale helicopter in presence of wind gusts," *International Journal of Control*, vol. 82, no. 12,

pp. 2206–2220, 2009.

[5] A. Martini, F. L*é*onard, and G. Abba, "Dynamic modelling and stability analysis of model-scale helicopters under wind gust," *Journal of Intelligent and Robotic Systems*, vol. 54, no. 4, pp. 647–686, 2008.

[6] M. L. Civita, G. Papageorgiou, W. C. Messner, and T. Kanade, "Design and flight testing of a high-bandwidth $\mathcal{H}_\infty$ loop shaping controller for a robotic helicopter," *Journal of Guidance, Control, and Navigation*, vol. 29, no. 2, pp. 485–494, 2006.

[7] C. D. Yang, W. H. Liu, and C. C. Kung, "Nonlinear $\mathcal{H}_\infty$ decoupling control for hovering helicopter," in *Proceedings of the American Control Conference*, vol. 6, pp. 4353–4358, May 2002.

[8] C. D. Yang and W. H. Liu, "Nonlinear $\mathcal{H}_\infty$ decoupling hover control of helicopter with parameter uncertainties," in *Proceedings of the American Control Conference*, vol. 4, (Denver, CO, USA), pp. 3454–3459, Jun. 2003.

[9] C. C. Kung, "Nonlinear $\mathcal{H}_\infty$ robust control for six DOF equations of motion of rigid body with mass uncertainty," in *Proceedings of the 17th World Congress, the International Federation of Automatic Control*, (Seoul, Korea), pp. 11346–11351, Jul. 2008.

[10] C. C. Luo, R. F. Liu, C. D. Yang, and Y. H. Chang, "Helicopter $\mathcal{H}_\infty$ control design with robust flying quality," *Aerospace Science and Technology*, vol. 7, no. 2, pp. 159–169, 2003.

[11] X. Yang, H. Pota, and M. Garratt, "Design of a gust-attenuation controller for landing operations of unmanned autonomous helicopters," in *18th IEEE International Conference on Control Applications*, (Saint Petersburg, Russia), pp. 1300–1305, Jul. 2009.

[12] M. A. Khalaf, J. Huang, and F. L. Lewis, *Nonlinear $\mathcal{H}_2/\mathcal{H}_\infty$ Constrained Feedback Control: A Practical Design Approach Using Neural Networks (Advances in Industrial Control)*. Springer, 2006.

[13] A. Isidori and A. Astolfi, "Disturbance attenuation and $\mathcal{H}_\infty-$control via measurement feedback in nonlinear systems," *IEEE transactions on automatic control*, vol. 37, no. 9, pp. 1283–1293, 1992.

[14] J. Huang and C. F. Lin, "Numercial approach to computing nonlinear H_∞ control laws," *Journal of Guidance, Control, and Dynamics*, vol. 18, no. 5, pp. 989–994, 1995.

[15] G. D. Padfield, *Helicopter Flight Dynamics: the Theory and Applications of Flying Qualities and Simulation Modelling, 2nd edition*. Blackwell Publishing, 2007.

[16] K. M. Zhou, J. C. Doyle, and K. Glover, *Robust and Optimal Control*. Upper Saddle River: Prentice Hall, 1995.

[17] M. A. Garratt, *Biologically Inspired Vision and Control for an Autonomous Flying Vehicle*. PhD

thesis, Australian National University, Australia, Oct. 2007.

[18] B. Ahmed, H. Pota, and M. Garratt, "Flight control of a rotary wing UAV using backstepping," *International Journal of Robust and Nonlinear Control*, vol. 20, no. 6, pp. 639–658, 2010.

TABLE II

PARAMETERS OF THE VARIO HELICOPTER

Parameters	Value
a_{mr}: Main rotor blade 2D lift curve slope	5.7
A_l: Lateral cyclic to main rotor pitch ratio	$-0.17\ rad/ms$
B_l: Longitudinal cyclic to main rotor pitch ratio	$-0.19\ rad/ms$
C_l: Longitudinal cyclic to flybar pitch ratio	$-1.58\ rad/ms$
D_l: Lateral cyclic to flybar pitch ratio	$-1.02\ rad/ms$
c_{mr}: Main rotor blade chord	$0.076\ m$
c_{tr}: Tail rotor blade chord	$0.043\ m$
C_{D_0}: Profile drag coefficient	0.012
D_{mx}: Horizontal distance between main rotor and $y-$axis	$0.036\ m$
D_{my}: Sideways distance between main rotor and $x-$axis	$-0.0029\ m$
D_{mz}: Vertical distance between main rotor and horizontal plane	$-0.3321\ m$
D_{tx}: Horizontal distance between tail rotor and $y-$axis	$-1.4440\ m$
D_{ty}: Sideways distance between tail rotor and $x-$axis	$-0.0029\ m$
D_{tz}: Vertical distance between tail rotor and horizontal plane	$1.1379\ m$
I_{xx}: Moment of inertia about $x-$axis	$12.3\ kgm^2$
I_{yy}: Moment of inertia about $y-$axis	$18.7\ kgm^2$
I_{zz}: Moment of inertia about $z-$axis	$6.6\ kgm^2$
I_{xz}: Product of inertia	0
k_{ind}: Induced power correction factor	1.2
K_s: Flybar to main rotor pitch mixing ratio	0.8
k_β: center-spring rotor stiffness	$1165.7\ N/m$
M_a: All-up weight	$27.738\ kg$
N_b: Number of main rotor blades	3
R_b: Main rotor radius	$1.25\ m$
S_{fus}^X: Fuselage equivalent flat plate area in $x-$direction	$-0.036\ m^2$
S_{fus}^Y: Fuselage equivalent flat plate area in $y-$direction	$0.0029\ m^2$
S_{fus}^Z: Fuselage equivalent flat plate area in $z-$direction	$-0.6379\ m^2$
κ_b: Profile drag power correction factor	4.7
Ω: Main rotor angular velocity	$89.01\ rad/sec$
Ω_{tr}: Tail rotor angular velocity	$481.55\ rad/sec$